Impact-crater ejecta on Bennu indicate a surface with very low strength

Mark Perry (mark.perry@jhuapl.edu)
The Johns Hopkins University Applied Physics Laboratory https://orcid.org/0000-0003-1600-6856

Olivier Barnouin
Johns Hopkins University Applied Physics Laboratory https://orcid.org/0000-0002-3578-7750

Ronald Daly
Johns Hopkins University Applied Physics Laboratory https://orcid.org/0000-0002-1320-2985

Edward Bierhaus
Lockheed Martin (United States)

Ronald-Louis Ballouz
University of Arizona https://orcid.org/0000-0002-1772-1934

Kevin Walsh
Southwest Research Institute https://orcid.org/0000-0002-0906-1761

Michael Daly
York University https://orcid.org/0000-0002-3733-2530

Daniella DellaGiustina
Lunar and Planetary Laboratory, University of Arizona https://orcid.org/0000-0002-5643-1956

Michael Nolan
University of Arizona https://orcid.org/0000-0001-8316-0680

Josh Emory
Northern Arizona University

Manar Al Asad
University of British Columbia https://orcid.org/0000-0001-8209-858X

Catherine Johnson
University of British Columbia

Carolyn Ernst
JHUAPL

Erica Jawin
Smithsonian National Museum of Natural History

Patrick Michel
Université Côte d'Azur, Observatoire de la Côte d'Azur, CNRS, Laboratoire Lagrange
https://orcid.org/0000-0002-0884-1993

Dathon Golish
University of Arizona https://orcid.org/0000-0002-6159-539X

William (Bill) Bottke
Southwest Research Institute https://orcid.org/0000-0002-1804-7814
Jeffrey Seabrook
York Universirty https://orcid.org/0000-0002-2163-7276
Dante Lauretta
Lunar and Planetary Laboratory, University of Arizona

Article

Keywords: planetary science, comets, asteroids, earth and environmental science

Posted Date: July 16th, 2021

DOI: https://doi.org/10.21203/rs.3.rs-426688/v1

Impact-crater ejecta on Bennu indicate a surface with very low strength

M.E. Perry[1], O.S. Barnouin[1], R.T. Daly[1], E.B. Bierhaus[2], R.-L. Ballouz[3], K.J. Walsh[4], M.G. Daly[5], D.N. DellaGiustina[3], M.C. Nolan[3], J.P. Emery[6], M.M. Asad[7], C.L. Johnson[7], C.M. Ernst[1], E.R. Jawin[8], P. Michel[9], D.R. Golish[3], W.F. Bottke[4], J. Seabrook[5], and D.S. Lauretta[3].

[1]Johns Hopkins University Applied Physics Laboratory, Laurel, MD, USA (mark.perry@jhuapl.edu), [2]Lockheed Martin Space, Littleton, CO, USA, [3]Lunar and Planetary Laboratory, University of Arizona, Tucson, AZ, USA, [4]Southwest Research Institute, Boulder, CO, USA, [5]York University, Toronto, Canada, [6]Northern Arizona University, Flagstaff, AZ, USA, [7]University of British Columbia, Vancouver, Canada, [8]National Museum of Natural History, Smithsonian Institution, Washington, DC, USA. [9]Université Côte d'Azur, Observatoire de la Côte d'Azur, CNRS, Laboratoire Lagrange, Nice, France

Abstract

A planetary surface's resistance to change is generally described as its "strength" (units of stress). The surface strength of small, rubble-pile asteroids, which consist of fragments of larger bodies that were collisionally disrupted, is poorly constrained due to their wide departure from terrestrial analogs. Here, we report the observation of an ejecta deposit surrounding an impact crater that limits the maximum surface strength of the near-Earth rubble-pile asteroid (101955) Bennu. The presence of this deposit implies that ejecta were mobilized with velocities less than the escape velocity of Bennu, 20 cm/s. Because ejecta velocities increase with surface strength, the ejecta deposit can only be explained if the effective strength of the surface material near the crater is exceedingly low, ≤100 Pa. This is three orders of magnitude below values commonly used for asteroid surfaces, but is supported by previous observations of an artificial impact crater on a similar asteroid, Ryugu. Our findings indicate a mobile surface that has likely been renewed multiple times since Bennu's initial assembly and have far-reaching implications for interpreting observations of Bennu and other rubble piles.

Features on the surface of a planetary body reflect its evolution, impact history, degradation processes, and material properties. Of particular importance to interpreting remote observations of such bodies is the surface's resistance to mechanical changes, represented by a group of properties described as "strength" and having units of stress. Using only Earth-based observations, determining the surface strength of a distant asteroid is challenging, especially in the case of small, rubble-pile asteroids that consist of gravitationally bound and unconsolidated fragments of collisionally disrupted precursors. In such cases, it has been common to assume a surface strength >100,000 Pa, typical of weakly cemented basalt [1] and lunar regolith [2].

The Hayabusa2 and OSIRIS-REx (Origins, Spectral Interpretation, Resource Identification and Security–Regolith Explorer) missions to the rubble-pile asteroids Ryugu [3] and Bennu [4,5], respectively, have offered the opportunity to better constrain surface strength via spacecraft data acquired in proximity. OSIRIS-REx observations have shown that meter-scale boulders on Bennu's surface have an estimated strength of 0.1 to 1.7 MPa [6,7], but this does not tell us about the inter-particle cohesive strength that is relevant for loose regolith found on rubble-pile asteroids. Analyses of Hayabusa2's Small Carry-on Impactor (SCI) experiment [8] on Ryugu suggest an exceptionally low surface strength of <1.3 Pa on the basis of a 15-m-diameter artificially created crater. However, it has not been clear whether the low strength implied from this single experimental outcome can be extrapolated to larger craters, to the global surface of Ryugu, or to other asteroids. Here we investigate the surroundings of a larger, naturally created impact crater on Bennu, with implications for the strength of the surface and the generalizability of the SCI experimental result from Ryugu.

An ejecta field on Bennu

We observed an unusually smooth, homogenous area surrounding and downslope (north) of the 70-m-diameter Bralgah Crater, centered at 45°S, 325°E (Fig. 1) in images acquired by the OSIRIS-REx Camera Suite (OCAMS) [9–11]. The terrain is the largest photometrically distinct and smooth area on Bennu, encompassing approximately 0.024 km^2 or 6% of the southern hemisphere. In multispectral images, the color of the crater and the surrounding smooth area is more homogenous than that of the rest of Bennu's surface, which varies at the scale of boulders (meters to tens of meters)[12]. This region shows a distinct b′/v normalized band ratio > 1, which is typical for smoother and younger (as inferred from space-weathering trends) terrains on Bennu (Fig. 1d, S3). The surface is smoother by a factor of 2 than the Bennu average, as determined by measures of roughness such as variations in slope over length scales of 1 to 5 m [13] and tilt variation (Fig. 1c). There are two boulders to the northeast (Fig. 1a), behind which the terrain distal to radially from the crater is rockier and 2 to 5 m lower (Fig. S1).

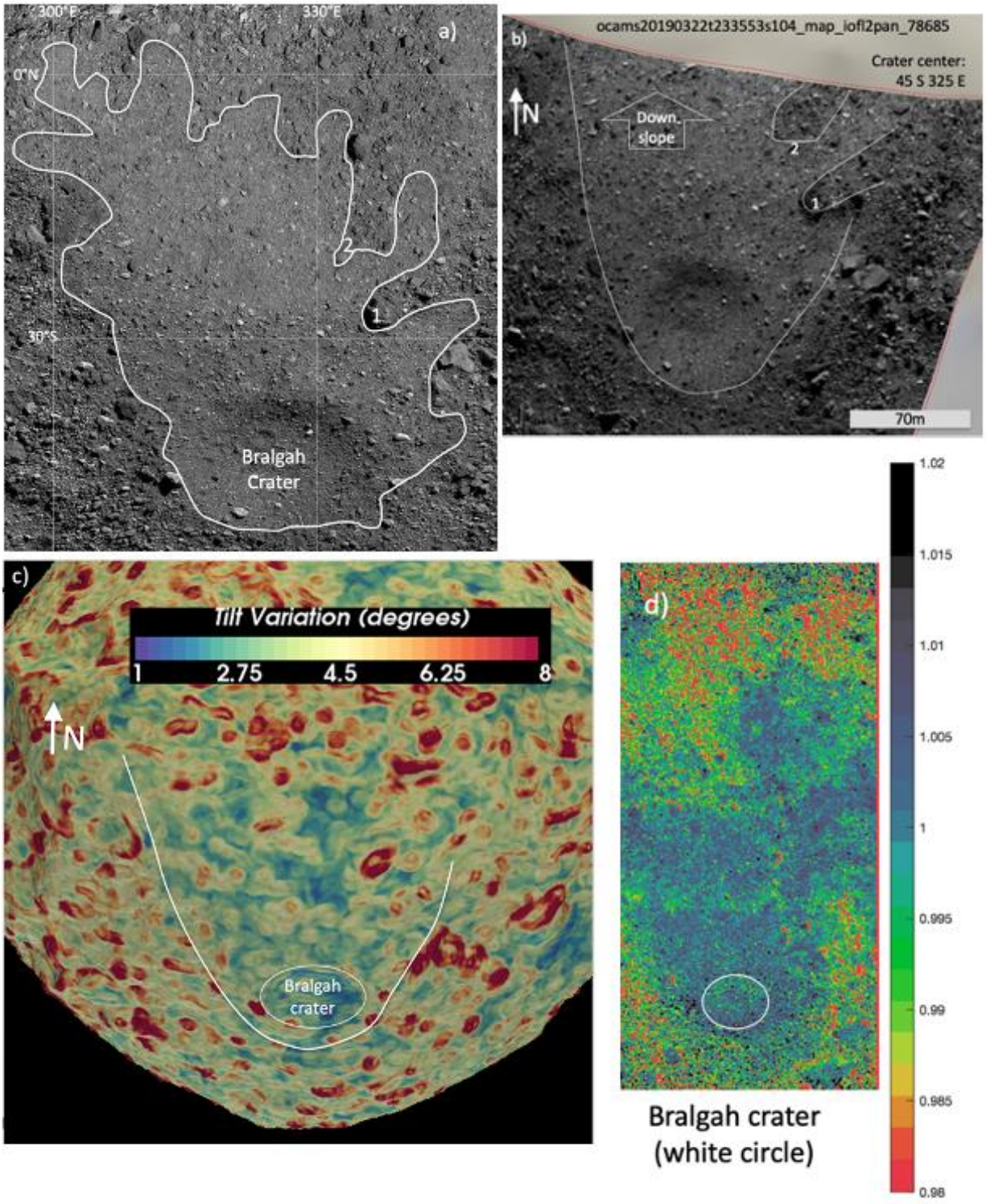
300°E
330°E
a)
0°N
30°S
1
2
Bralgah
Crater
b)
ocams20190322t233553s104_map_iofl2pan_78685
Crater center:
45 S 325 E
N
Down-
slope
2
1
70m
c)
Tilt Variation (degrees)
1
2.75
4.5
6.25
8
N
Bralgah
crater
d)
Bralgah crater
(white circle)
1.02
1.015
1.01
1.005
1
0.995
0.99
0.985
0.98

Fig. 1. Bralgah Crater and the surrounding uniform terrain. **a**, OCAMS/PolyCam mosaic [11] showing the uniform terrain (white border) northward of and surrounding the 70-m-diameter crater. The terrain northeast of the two rocks labeled 1 and 2 (20°S, 333°E and 28°S, 337°E) is rougher and darker. The top of this image is just north of the equator, where elevations are lowest on Bennu. The terrain is rougher, with more boulders than to the south. **b**, A single OCAMS/MapCam image (image ID shown at top) with a smoothed white line demarcating the distinctive terrain. **c**, Tilt variation, a measure of surface roughness, showing the range of surface slopes within the local area. **d**, The b′/v band ratio map for 300°E to 0°E and 60°S to 60°N. Bralgah Crater and the surrounding terrain have higher ratios. Previous work indicates that high b′/v band ratios seem to be associated with younger, smoother terrains on Bennu, including those that might have experienced recent mass movement [12].

The crater itself is fully encircled by a well-defined, raised rim and has a slightly asymmetric bowl-shaped interior [14]. From among similarly sized craters on Bennu [14], Bralgah Crater's morphology is most reminiscent of classical simple craters on larger bodies such as Earth's Moon. The well-defined topographic expression and morphology suggest that Bralgah Crater has undergone little degradation [14]. It has a depth-diameter ratio of 0.07 ± 0.01 with respect to elevation and a volume of 9×10^3 m^3 ±50% [14]. The crater resides on a ~23° regional slope (Fig. S4 shows the detailed topography). The northern crater wall has a steeper slope than the southern wall, which has more large boulders.

Buried structures near the surface can complicate crater formation [8,14], but there is little evidence of this at Bralgah Crater. Its circular rim and relatively smooth floor indicate that the near-surface material was initially uniform and did not contain large boulders or regions of higher strength to interfere with crater formation. To achieve this uniformity, the homogeneity of the near-surface material at the location of Bralgah Crater would need to extend to a depth of approximately a tenth of a crater diameter, or 7 m. Given the exceptionally rough and varied surface of Bennu [4], this homogeneity is initially surprising. However, it is supported by two other observations: 1) the crater is located in the southern hemisphere, where large boulders appear to effectively retain fine material, resulting in a rounder shape than in the north [15]; and 2) localized mass flows have excavated several meters of regolith from around large boulders on Bennu [16], suggesting a reservoir of mobile material.

Because the smooth, uniform terrain surrounds and inhabits the crater, we infer that they formed concurrently. A crater that post-dated the terrain would have roughness and color that differed from the surrounding terrain, and a crater that pre-dated the terrain would show evidence of infilling, particularly at the downslope crater wall, which would be shallower than the upslope wall, instead of steeper as we observe. We therefore conclude that the material that composes the uniform terrain is a product of or triggered by the cratering event.

Further, the uniform ring of terrain on and just beyond the rim uphill and to the south, east, and west (Fig. 1a) is best explained by material that left the crater in those directions rather than by mass wasting, which would create a more unilinear set of features (c.f.)[16,17]. We therefore infer that this terrain consists of ejecta from the impact that formed Bralgah crater.

Ejecta and surface strength

For ejecta to fall back onto Bennu's surface, the particles must be ejected at speeds lower than Bennu's escape velocity of 20 cm/s [18,19]. Impact-scaling relationships (Table 1), developed from terrestrial testing and combined with assumptions about impact velocity and material properties, enable parameters such as ejecta velocities to be estimated from the crater size [20,21]. The stronger and more cohesive the surface material, the higher the ejection velocities. Analyses of crater formation are parameterized in either a strength or gravity regime. (Armoring, when the impactor is smaller than the target particle, requires different analyses[22].) In the strength regime, surface strength controls the impact process, particularly the crater/impactor size ratio and the velocities of the ejecta. If strength is negligible, then ejecta velocities and the final crater size are controlled by gravity. For either regime, most mass is ejected late in crater formation from near the crater edge, where ejecta velocities are also lowest (Fig. 2b). The scaling relationship for a gravity-controlled impact can be simplified to $v=\sqrt{gR}$, where v is the ejection velocity for material near the crater edge, g is the local acceleration of gravity, and R is the final crater radius [21]. On Bennu, surface accelerations range from $5\text{x}10^{-5}$ m/s^2 at the equator to $8\text{x}10^{-5}$ m/s^2 at the poles [18]. For Bralgah Crater, at 45° S and with R = 35 m, v = ~4.5 cm/s at the crater edge, resulting in suborbital particle trajectories that re-impact Bennu within a crater diameter (Fig. 3).

On a slope, an ejecta deposit is asymmetric even for impacts that occur at near-normal incidence. Material ejected downslope would travel farther and land with a higher velocity component along the surface than material ejected in other directions. Material ejected upslope (south) would land with a velocity near normal incidence and have less than 1-cm/s velocity along the surface. Much of the ejecta on the upslope side of the crater would land closer to the upslope (southern) crater rim. Based on experiments such as those by Takizawa and Katsuragi et al. (2020) [23], upslope ejecta likely collapsed into the crater shortly after landing, contributing to the shallower slope of the southern crater wall.

Table 1. Scaling relationships for both gravity and strength regimes used for calculations and simulations of impact cratering and resulting ejecta [21]. R is the final crater radius; Y is a measure of surface strength (Pa); ρ is surface density; U, δ, and m respectively are impactor velocity, density, and mass; and x is the radial distance from the crater center. ν, μ, C_1, C_4, H_1, and H_2 are fitted constants.

Parameter	Values and Relationships
Crater radius (strength regime)	$R\left(\frac{\rho}{m}\right)^{1/3} = H_2\left(\frac{\rho}{\delta}\right)^{(1-3\nu)/3}\left[\frac{Y}{\rho U^2}\right]^{-\mu/2}$
Crater radius (gravity regime)	$R\left(\frac{\rho}{m}\right)^{1/3} = H_1\left(\frac{\rho}{\delta}\right)^{(2+\mu-6\nu)/[3(2+\mu)]}\left[\frac{ga}{U^2}\right]^{-\mu/(2+\mu)}$
Transition strength	$Y_t = \rho g a$ (The gravity regime applies when surface strength is less than Y_t; for Bennu, Y_t <1 Pa for a < 15 m)
Ejection velocity (strength regime)	$\nu\sqrt{\frac{\rho}{Y}} = C_3\left(\frac{x}{R}\right)^{-1/\mu}$ $C_3 = C_1\left((4\pi/3)^{1/3}H_2\right)^{-1/\mu}$ At the crater radius (x=R) simplifies to v~=$\sqrt{gR}$
Ejection velocity (gravity regime)	$\frac{\nu}{\sqrt{gR}} = C_2\left(\frac{x}{R}\right)^{-1/\mu}$ $C_2 = C_1\left((4\pi/3)^{1/3}H_1\right)^{-(2+\mu)/2\mu}$ At the crater radius (x=R) simplifies to v~=$\sqrt{Y/\rho}$
Mass ejected faster than v (strength regime)	$\frac{M(\nu)}{\rho R^3} = C_6\left(\nu\sqrt{\frac{\rho}{Y}}\right)^{-3\mu}$ $C_6 = C_4 H_2^{-3}$
Mass ejected faster than v (gravity regime)	$\frac{M(\nu)}{\rho R^3} = C_5\left(\frac{\nu}{\sqrt{gR}}\right)^{-3\mu}$ $C_5 = C_4(4\pi/3)^{-\mu/2}H_1^{-3(\mu+2)/2}$
Target parameters for sand [density and strength varied]	μ= 0.41, H_1= 0.59, H_2= 0.4, ν= 0.4, density (ρ)= [1,000 to 1,500] kg/m^3, Y=[0 to 100]
Impactor parameters, gravity regime [varied]	Density (δ)= [1,500 to 3,600] kg/m^3, U= [3,000 to 7,000] m/s, a= [0.17 to 1.3] m
Bennu parameters	GM= 4.93 m^3/s^2, rotation period= 4.3 hrs, shape model v42, steepest slopes = 40°

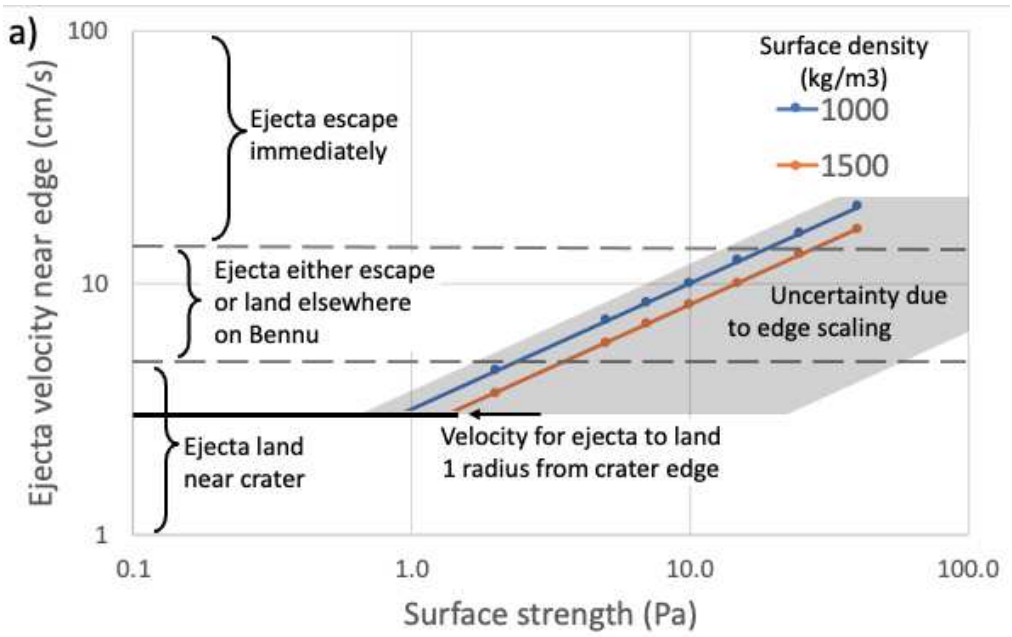

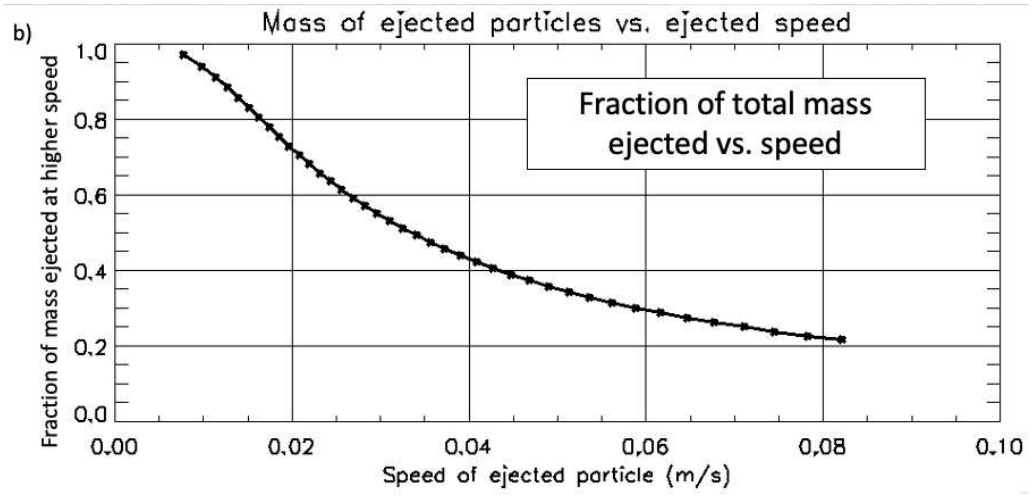

Fig. 2. a, Ejecta velocity vs. strength of Bennu's surface material to a depth of approximately 7 m. If the strength is greater than 100 Pa, then most of the ejecta, which are launched near the crater edge, will land either far from the crater or escape from Bennu. The shaded area represents the uncertainty in crater-forming processes at the crater edge in microgravity (see supplementary information). **b**, During a cratering event, most mass is ejected at lower speeds and near the crater edge. Using the size of Bralgah Crater and gravity-regime scaling, this plot shows the fraction of total ejected mass that has speeds below the plotted value. Only 20% of the ejected mass is ejected faster than 8 cm/s.

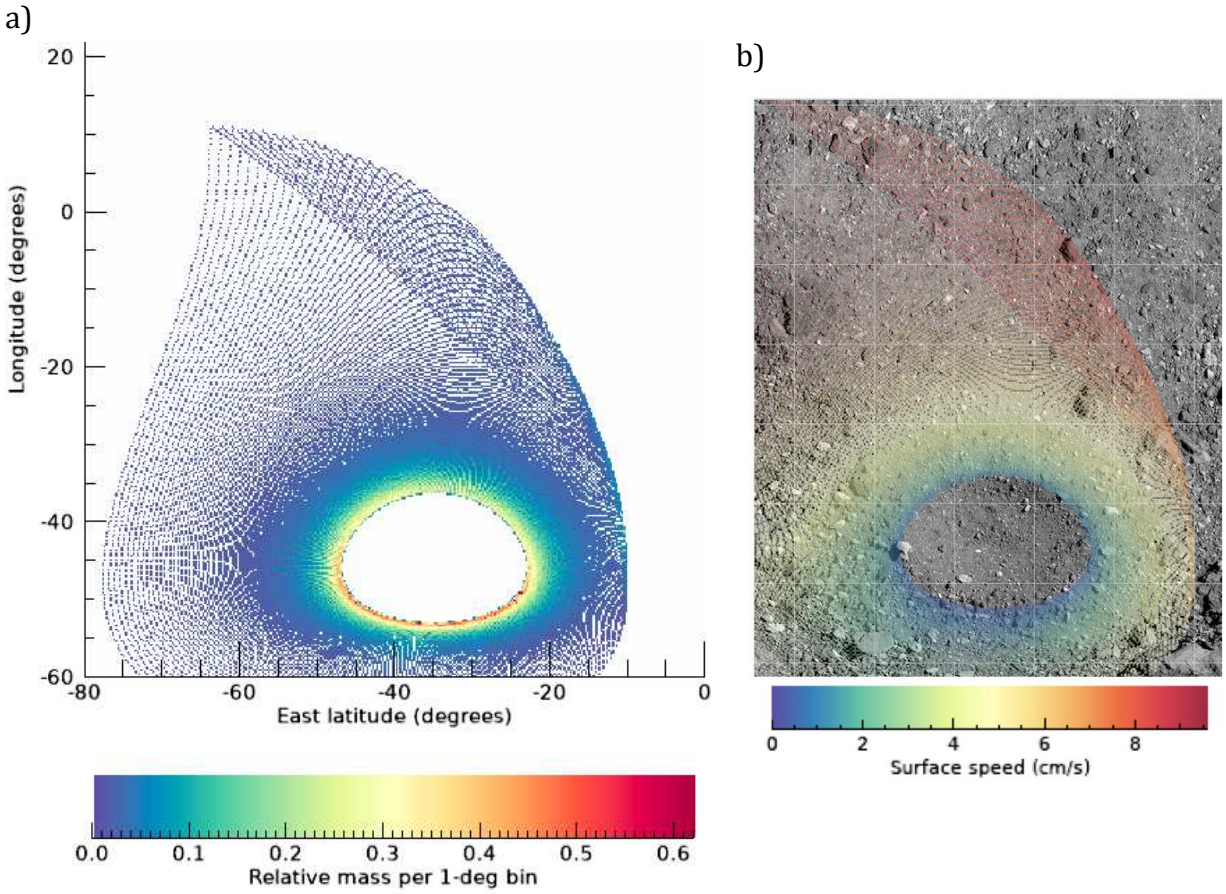

Fig. 3. Simulation results of ejecta leaving the rim of Bralgah Crater according to gravity scaling. **a**, Density map of the mass deposition. The north/south asymmetry is due to the regional slope and the westward curve is due to Bennu's rotation. **b**, Velocity map overlain onto a map of the Bralgah Crater region. Ejecta that returns to the surface within a distance of 1 crater radius to the north lands with a velocity <3.5 cm/s. Material ejected at speeds between 8 and 12 cm/s are omitted from the plots because their landed locations are widely dispersed over Bennu, and they make up less than 10% of the total ejected mass. Most material ejected at >12 cm/s does not return to Bennu.

Before the discovery of the Bralgah ejecta field, it had been reasonable to assume that all craters on Bennu formed in the strength regime because so little strength would be needed to exceed the influence of microgravity. In the strength regime, where surface material properties govern the cratering process, ejection velocities (Table 1) at the crater edge are approximated by $v=\sqrt{Y/\rho}$, where Y is a measure of strength with dimensions of stress and ρ is the surface density. To determine whether Bralgah crater formed in the strength or gravity regime, we examined the relationship between ejecta speeds and surface strength. Our analyses reveal that a miniscule surface strength of just 100 Pa would cause most material to leave the crater at higher than the ~3.5 cm/s velocities required for ejecta to land near the crater (Figs. 2 and S2). We therefore conclude that the surface strength of Bennu in the Bralgah Crater region must be <100 Pa, which is nearly strengthless.

This value is substantially below most material analogs used in crater studies. Typical dry soils on Earth and loose lunar soils have respective strengths of 180 kPa [1] and >520 Pa [24]. If these strength values existed on Bennu, the ejecta from Bralgah crater would have launched at velocities much higher than the asteroid's escape velocity. Thus, the presence of ejecta surrounding Bralgah Crater suggests that gravity-regime scaling is applicable to at least some areas of rubble-pile bodies. Our conclusion is consistent with the very low effective strength (<1.3 Pa) deduced from the SCI experiment on Ryugu by Hayabusa2 [8].

Evidence of surface mass flow

The depression in elevation behind (north of) boulder 2 (Fig. S1) is 4-to-5-m deep and provides an estimate of the thickness of the uniform terrain north and downhill of Bralgah Crater. If uniformly distributed over the region, material excavated from the crater can only account for 20–30 cm of that thickness. Moreover, the majority of ejecta would re-impact Bennu within 1 crater diameter from the rim (see the dense region near the crater rim in Fig. 3a). Insight into the source of this material comes from the fact that some of it appears to have flowed up to and around boulders 1 and 2 (Fig. 1). Ejecta deposition alone would have placed particles both atop and downslope of the boulders. Images show that material flowed north-northwest [16]as it piled against the boulders (Fig. S5). These observations suggest that a mass flow field added material to the extended ejecta blanket.

The flow field and ejecta blanket are likely related. Downslope ejecta would have re-contacted Bennu at relatively shallow angles of 25 to 30° to the surface and with velocities of 5 to 7 cm/s tangent to the surface (Fig. 3b). This velocity is sufficient to dislodge particles. For example, assuming that the scaling laws remain valid for impacts at very low speeds, a 10-cm-diameter ejecta particle returning to a strengthless surface at 5 cm/s would create a 40-cm-diameter crater and activate a volume of material 100 times that of the particle. The material in this area exhibits a surface slope greater than 20° at Bennu's current rotation rate (Barnouin et al. in prep). This high slope angle suggests that the surface is marginally stable, and the returning ejecta would have been sufficient to supply what little impetus is required to initiate a downhill flow.

Downslope flow has characteristics of a gravity current or inertial-debris flow, a granular flow composed of intensively colliding particles [25]7/16/2021 9:45:00 AM. Inelastic collisions of flowing particles and their plunge into the regolith provide momentum transport that entrains surface particles similar to a powder-snow avalanche and different from landslides that are slumps or translational slides and do not engage as much underlying material. Inertial-debris flows may produce lobes, and we observe several such features at the northward (equatorial) terminus (Fig. 1b), with possible extension past the equator. For a portion of the field, no sharp demarcation is evident, which may be due to the flowing material slowing and thinning as it reaches the lower slopes near the equator. Large boulders are sometimes found at the terminus of mass wasting; the east-west cluster of boulders from 0 to 8N latitude may be such a collection (Fig. 1a). The lack of boulders larger than a few meters in the uniform terrain suggests that larger boulders have been removed or buried.

Static and dynamic friction angles in collections of particles supply coefficients that are useful for determining equivalent friction and its effect on flow. Bennu's steeper regional slopes are less than 40° [26], which is an upper bound for cohesionless material. Using 40° to represent the static friction angle, the estimated dynamic friction is approximately 10° shallower (30°) and corresponds to a coefficient of dynamic friction of 0.58 [27]. Applying this friction coefficient to the material disturbed by the returning ejecta, a flow that started with a velocity of 5 cm/s would travel along a 20° slope more than 100 m, the distance to the equator, before being stopped by friction. A slightly lower dynamic friction angle of 25° requires only 3.5 cm/s initial velocity to reach the equator. Acceleration due to the slope is possible. For material moving at an angle to the slope, there is a slight downslope acceleration, but this has a small effect on the original velocity for material within 45° of the downslope direction.

With insufficient material available from the crater, most of the flow field must consist of existing, marginally stable material that was mobilized and remixed, eliminating the need for a large source region. The observed terrain is a mixture of ejecta and pre-existing regolith creating the layer.

The ejecta-initiated flow must have been sufficiently massive to scour the surface over which it passed, removing unanchored rocks and boulders and leaving the relatively smooth, homogenous terrain that we observe. The lack of tracks from rolling boulders is not surprising if all of the material flowed together. Filling of low areas contributed to the observed smoothness of the terrain. Boulders 1 and 2 in Fig. 1 were too large or too deeply embedded to be dislodged. Disrupted material continued moving until it encountered an obstacle that it could not dislodge or reached the equatorial region, where elevation is lowest. The lack of secondary craters, which would normally be present around a large crater, is further corroboration of displacement due to flowing material.

A distinguishing characteristic of the event that created Bralgah Crater is that the impact occurred into a deep reservoir of finer material. Most large craters on Bennu have rocky floors [14], so gravity-scaled crater formation would have transitioned to the strength regime when encountering a coherent subsurface. The low ejection speeds that enabled retention in the case of the crater we studied would not have occurred. Combined with the information

gleaned from the Hayabusa2 SCI experiment, a reasonable conclusion is that near-surface fine material is essentially strengthless if not always thick.

There are no other obvious, large ejecta fields on Bennu. Bralgah Crater is the only crater on Bennu with several of the necessary characteristics: large size (to provide sufficient material), mid-latitude location (because material flows down toward the equator), impact into a deep layer of fine material (maintain gravity regime for the entire crater-forming event), and relative youth for a crater of its size (so that the field has not been overprinted and masked by subsequent surface processes). The flow field is highly visible because of the avalanche caused by the reaccreted ejecta. Most other large craters on Bennu are near or on the equator, so ejected material is already at low elevation and lands with negligible surface velocity. There are a few other large candidate craters at high latitude, but they appear older and degraded [17], and it is possible that any associated ejecta or flow fields are weathered or disturbed past recognition.

Implications of a low-strength surface

Resurfacing of a body with a strengthless surface is much faster than for a high-strength surface. For the same population of impactors, crater radii in a strengthless surface are 10 times as large—involving 100 times the area and 1,000 times the volume—than surfaces responding in a strength regime with Y~0.2 MPa. This large difference in scale is then enhanced by ejecta retention: the low ejection velocities produced by impacts into low-strength surfaces return ejected material to the surface, modifying the top layer of the asteroid and infilling craters. From the ejecta-velocity equations (Table 1), most ejecta from impacts on Bennu are retained. For Bralgah Crater, >80% of the ejecta did not escape (Figs. 3, S2). Possibly the most important consequence for rubble-pile asteroids is that their typically high spin rates [28] create steep slopes where material is readily mobilized by ejecta re-impacting the surface. For the impact that created Bralgah crater, the area resurfaced by the induced flow is 50 times the area of the crater.

We estimate the size of the impactor that made Bralgah Crater by first using the gravity-regime parameterizations. Using the range of values in Table 1, the impactor had a radius, a, between 0.17 and 0.45 m for velocities in the main belt. Contributing most to the range of sizes are the velocity of the impactor and the density uncertainties. If Bennu's near-surface material has the 100 Pascals of strength as permitted by the analyses of the minimum observed ejecta velocity, then the impactor could have a radius as large as 1.3 m according to the strength-regime parameterization. This radius is a factor of 4 smaller than the 5.3-m radius required for a dry-soil strength of 0.18 MPa, which was used in a previous analysis of. Bennu's surface [17].

Impactor sizes relate to crater-retention age through the modeled impactor flux, which has a size-frequency distribution that varies approximately by the inverse cube of the size of the impactor [29]. The 0.18 MPa assumption for surface strength correlates to a crater-retention age of 0.1 to 1 Gyr, under the condition that Bennu is drifting within the main asteroid belt. If the surface strength is lower such that the impactors were a factor of 4 smaller, the impactor flux would be 64 times higher (several per million years [22]) and correlate to an age

that is younger by the same factor. However, this simple scaling ignores several complicating factors. Bennu may have become collisonally decoupled from the main belt within the last 1.75± 0.75 Myr[29], so these derivations, based on the main-belt environment, must be modified for the much lower flux and higher speeds of impactors in near-Earth space. Also, there are observations of competency at several meters below the surface on both Bennu and Ryugu (14, 30, 8). These increases in strength reduce the size of craters and consequently increase the estimates of age beyond the assumption of universal gravity scaling. No subsurface competent layer is seen at Bralgah Crater, which probed at least 7 m below the surface. The low strength of Bennu's upper layer leads to low ejecta velocities and fine-material retention regardless of possible cohesiveness in deeper layers. The apparent deep internal stiffness of Bennu [15,26,31] may have little effect on the recent cratering record. Given the varied surfaces found on Bennu, a single relationship between impactor size and crater diameter may not exist.

A companion paper [22] compared analyses with different assumptions for surface characteristics to the size frequency distribution of Bennu's craters and deduced the crater-retention ages of Bennu. Justified by the findings presented here and by the analyses of the Hayabusa2 SCI experiment, the authors included assumptions gravity and low-strength regimes. The deduced impactor sizes are smaller and the crater-retention ages are younger than previous estimates. Given Bennu's estimated formation age of approximately 1 Gyr inferred from possible asteroid-source families in the main belt [32,33], Bennu has likely been resurfaced multiple times.

The evidence of retained ejecta on Bennu's surface provides an unexpected route toward understanding the strength of the top layer of material on a rubble-pile asteroid. Further, our analysis of Bralgah Crater on Bennu, together with Hayabusa2's artificial cratering experiment on Ryugu, offer two measurements of negligible cohesive strength on two different rubble-pile asteroids and from craters of two different diameters (70 versus 15 m), indicating a potentially broad applicability to rubble-pile surfaces.

Three implications of this work indicate that resurfacing rates for rubble-pile asteroids are higher than for larger asteroids: (1) Due to the low strength of regolith, craters are larger than predicted by models that assume higher strength, so the same impactor flux overturns more of the surface. Taking this into account leads to reduced estimates of crater-retention age [22]. (2) Also due to the low strength, much of the crater material is ejected at velocities below the escape velocity, retaining the shock-comminuted material and contributing to crater infilling and other resurfacing. (3) With the high slopes available on fast-spinning asteroids, ejecta that return to the surface can easily mobilize material and create mass wasting that affects a larger area than the crater and ejecta-impact locations would alone. This work thus demonstrates that the microgravity environment on small rubble-pile asteroids results in distinct planetary geological processes.

372 **References**
373
374 1. Holsapple, K. A. The scaling of impact processes in planetary sciences. *Annual Review of*
375 *Earth and Planetary Sciences* **21**, 333–373 (1993).
376 2. Melosh, H. J. *Impact cratering: A geologic process*. (1989).
377 3. Sugita, S. *et al.* The geomorphology, color, and thermal properties of Ryugu: Implica-
378 tions for parent-body processes. *Science* **364**, (2019).
379 4. Lauretta, D. S. *et al.* The unexpected surface of asteroid (101955) Bennu. *Nature* **568**,
380 55–60 (2019).
381 5. Lauretta, D. S. OSIRIS-REx at Bennu: Overcoming Challenges to Collect a Sample of the
382 Early Solar System, in Sample Return Missions. *Elsevier, in press* (2021).
383 6. Rozitis, B. *et al.* Asteroid (101955) Bennu's weak boulders and thermally anomalous
384 equator. *Science Advances* **6**, (2020).
385 7. Ballouz, R. L. *et al.* Bennu's near-Earth lifetime of 1.75 million years inferred from cra-
386 ters on its boulders. *Nature* (2020) doi:10.1038/s41586-020-2846-z.
387 8. Arakawa, M. *et al.* An artificial impact on the asteroid 162173 Ryugu formed a crater in
388 the gravity-dominated regime. *Science* (2020) doi:10.1126/science.aaz1701.
389 9. Rizk, B. *et al.* OCAMS: The OSIRIS-REx Camera Suite. *Space Sci Rev* **214**, 26 (2018).
390 10. Golish, D. R. *et al.* Ground and In-Flight Calibration of the OSIRIS-REx Camera Suite.
391 *Space Sci Rev* **216**, 12 (2020).
392 11. Bennett, C. A. *et al.* A high-resolution global basemap of (101955) Bennu. *Icarus* 113690
393 (2020) doi:10.1016/j.icarus.2020.113690.
394 12. DellaGiustina, D. N. *et al.* Variations in color and reflectance on the surface of asteroid
395 (101955) Bennu. *Science* eabc3660 (2020) doi:10.1126/science.abc3660.

13. Barnouin, O. S. *et al.* Digital terrain mapping by the OSIRIS-REx mission. *Planetary and Space Science* **180**, 104764 (2020).
14. Daly, R. T. *et al.* The morphometry of impact craters on Bennu. *Geophysical Research Letters* **n/a**, e2020GL089672 (2020).
15. Daly, M. G. *et al.* Hemispherical differences in the shape and topography of asteroid (101955) Bennu. *Science Advances* **6**, eabd3649 (2020).
16. Jawin, E. R. *et al.* Global Patterns of Recent Mass Movement on Asteroid (101955) Bennu. *J Geophys Res-Planet* **125**, (2020).
17. Walsh, K. J. *et al.* Craters, boulders and regolith of (101955) Bennu indicative of an old and dynamic surface. *Nature Geoscience* **12**, 242–246 (2019).
18. Scheeres, D. J. *et al.* The dynamic geophysical environment of (101955) Bennu based on OSIRIS-REx measurements. *Nat Astron* **3**, 352–361 (2019).
19. Chesley, S. R. *et al.* Trajectory Estimation for Particles Observed in the Vicinity of (101955) Bennu. *J Geophys Res-Planet* **125**, (2020).
20. Housen, K. R., Schmidt, R. M. & Holsapple, K. A. Crater ejecta scaling laws: Fundamental forms based on dimensional analysis. *J. Geophys. Res.* **88**, 2485–2499 (1983).
21. Housen, K. R. & Holsapple, K. A. Ejecta from impact craters. *Icarus* **211**, 856–875 (2011).
22. Bierhaus, E. B., Trang, Daly, Bennett, & Barnouin. Crater size-frequency distribution on Bennu reveals impact armoring and young surface. *Nature Geoscience* (2021).
23. Takizawa, S. & Katsuragi, H. Scaling laws for the oblique impact cratering on an inclined granular surface. *Icarus* **335**, 113409 (2020).

418 24. Slyuta, E. N. Physical and mechanical properties of the lunar soil (a review). *Sol Syst Res*
419 **48**, 330–353 (2014).
420 25. McCaffrey (ed), W. D. *Particulate Gravity Currents*. vol. 31 (Blackwell Science Ltd.,
421 2001).
422 26. Barnouin, O. S. *et al.* Shape of (101955) Bennu indicative of a rubble pile with internal
423 stiffness. *Nature Geoscience* **12**, 247–252 (2019).
424 27. Iverson, R. M. The physics of debris flows. *Reviews of Geophysics* **35**, 245–296 (1997).
425 28. Vokrouhlický, D., Bottke, W. F., Chesley, S. R., Scheeres, D. J. & Statler, T. S. The Yarkov-
426 sky and YORP Effects. in *Asteroids IV* (ed. Michel, P.) (Univ. of Arizona, Tucson, 2015).
427 29. Bottke, W. F. *et al.* Interpreting the Cratering Histories of Bennu, Ryugu, and Other
428 Spacecraft-explored Asteroids. *AJ* **160**, 14 (2020).
429 30. Bierhaus, E. B. *et al.* Detailed Characterization of Crater Types and Relationships to Sur-
430 face and Sub-Surface Structure on Bennu. **51**, 2156 (2020).
431 31. Roberts. Rotational states and shapes of Ryugu and Bennu Implications for interior
432 structure and strength. *Planetary and Space Science* (2021).
433 32. Bottke, W. F. *et al.* In search of the source of asteroid (101955) Bennu: Applications of
434 the stochastic YORP model. *Icarus* **247**, 191–217 (2015).
435 33. Walsh, K. J., Delbo, M., Bottke, W. F., Vokrouhlicky, D. & Lauretta, D. S. Introducing the
436 Eulalia and new Polana asteroid families: Re-assessing primitive asteroid families in the
437 inner Main Belt. *Icarus* **225**, 283–297 (2013).
438 34. Daly, M. G. *et al.* The OSIRIS-REx Laser Altimeter (OLA) Investigation and Instrument.
439 *Space Sci Rev* **212**, 899–924 (2017).

35. Schultz, P. H., Ernst, C. M. & Anderson, J. L. B. Expectations for Crater Size and Photometric Evolution from the Deep Impact Collision. *Space Sci Rev* **117**, 207–239 (2005).

36. Housen, K. R., Sweet, W. J. & Holsapple, K. A. Impacts into porous asteroids. *Icarus* **300**, 72–96 (2018).

37. Rizk, B., D'Aubigny, C. D., DellaGiustina, D. N., Golish, D. & Laurentta, D. S. Origins, Spectral Interpretation, Resource Identification, Security, Regolith Explorer (OSIRIS-REx): OSIRIS-REx Camera Suite (OCAMS) bundle,. (2019).

38. Golish, D. R. *et al.* A high-resolution normal albedo map of asteroid (101955) Bennu. *Icarus* 114133 (2020) doi:https://doi.org/10.1016/j.icarus.2020.114133.

Acknowledgments: This material is based upon work supported by NASA under Contracts NNM10AA11C and NNG12FD66C, issued through the New Frontiers Program. The OSIRIS-REx Laser Altimeter and the Canadian authors were supported by the Canadian Space Agency. P.M. acknowledges funding support from the French space agency CNES, from the European Union's Horizon 2020 research and innovation program under grant agreement No. 870377 (project NEO-MAPP) and from Academies of Excellence: Complex systems and Space, environment, risk, and resilience, part of the IDEX JEDI of the Université Côte d'Azur. This work used the Small Body Mapping Tool (http:// sbmt.jhuapl.edu). We are grateful to the entire OSIRIS-REx Team of engineers, operators, scientists, and administrators for making the encounter with Bennu possible.

Author contributions:

M.E.P. led the data analysis and writing. O.S.B. led the Altimetry Working Group that produced the digital terrain models (DTMs). O.S.B, R.T.D., and C.M.E. contributed analyses and expertise on crater processes. M.G.D. and J.S. provided the altimetry data for the high-resolution DTMs. E.E.B. and R-L.B. provided analyses on crater-retention age. K.J.W., M.C.N., and P.M. contributed to writing. D.N.D and D.R.G. provided image and spectral analyses. J.P.E, M.M.A, E.R.J., W.F.B., and C.L.J. provided analytical insight. D.S.L. is principal investigator of the OSIRIS-REx mission.

Methods

Mapping and measurements

We mapped the ejecta blanket and flow field on a global OCAMS/PolyCam mosaic of Bennu with a pixel scale of ~5 cm/pixel [11] (Fig. 1a) and on OCAMS/MapCam image ocams20190322t233553s104_map_iofl2pan_78685 (Fig. 1b), which was collected on 22 March 2019 and has a pixel scale of 0.29 m/pixel. Elevations, slopes, and tilts are from SPC shape models [13]. Tilt variation (Fig. 1c) for a facet is the 1σ standard deviation of tilts of facets within a 5-m radius. Tilt variations are from the SPC v20 shape model; other elevations and slopes are from the SPC v42 shape model. The b′/v band ratio map in Fig. 1d was extracted from the global map in DellaGiustina et al. 2020[12]. The high-spatial-resolution local digital terrain models (DTMs) in Fig. S1 and S4 are produced from OSIRIS-REx Laser Altimeter (OLA) data[13,34].

Ejecta simulations

The high-fidelity numerical simulation (Figs. 3, S2) used IDL to understand the ejecta patterns and mass deposition. The velocities and mass distribution of ejecta are derived from terrestrial experiments, and Bennu parameters are derived from OSIRIS-REx observations (Table 1 contains the values and equations used). The simulation assumes gravity-regime scaling and Bennu's current shape and rotation rate. Ejecta particles are launched in a uniform distribution around the edge of Bralgah Crater and tracked in inertial space until they contact Bennu's surface. On the basis of terrestrial testing, all particles are ejected at 45° from local surface with a uniform azimuthal distribution. Higher order (two and above) gravity terms and mass concentrations are ignored as they have little effect on the modeled trajectories. The maximum ejection speed in the simulation is 8 cm/s. Higher-velocity particles have a low fraction of the total ejected mass, and they travel far from the crater because they approach escape velocity. During the time aloft, downslope ejecta underwent a 30-m drift westward due to Bennu's rotation. The crater formed slowly over twenty minutes, which was also the time aloft for most of the ejecta that returned to the surface. These parameterizations are based on crater diameter and are consistent with the outcome of the Hayabusa2 SCI experiment.

Applicability of gravity-regime scaling for Bennu's microgravity environment

Applying laboratory-based scaling relationships (Table 1) to Bennu necessitates extrapolating experimental results by several orders of magnitude. Nevertheless, the calculated ejection velocities are plausible and produce a feasible explanation for the ejecta field. These laboratory-based, point-source scaling relationships also proved relevant to full-scale experiments such as Deep Impact [35] and the SCI experiment [8]. Target compaction can suppress ejecta during impacts into porous targets [36], but the impactor creating Bralgah Crater was too small to cause compaction

Data availability

OCAMS data are available via the Planetary Data System (PDS) at https://sbn.psi.edu/pds/resource/orex/ocams.html[37]. The global image mosaic of Bennu is available in Bennett et al. (2020). OLA data underlying the DTMs used for slope calculations are available via the PDS at https://sbn.psi.edu/pds/resource/orex/ola.html (Daly et al.

2019). The v42 global shape model is available from the Small Body Mapping Tool (SBMT) at sbmt.jhuapl.edu. The ejecta-simulation programs and output are archived at https://lib.jhuapl.edu/.

Other potential flow fields on Bennu

The terrain surrounding and north of Bralgah Crater is not unique: some smaller areas on Bennu have similar smoothness, dearth of larger rocks, and comparable colors [12,38]. These other regions contain finer material and include the interior of some craters and possible flow fields unassociated with craters but on higher slopes that cover smaller areas. Steepening of the slopes by increased rotation rate, a small impact, or some other disturbance could have initiated an avalanche. Many of these regions are located near the same areas that have evidence of mass wasting surrounding large boulders [16]. Terraces (Barnouin et al. in prep) are additional indicators that much of Bennu's surface material in the middle latitudes is near its stability limit. In the northern hemisphere, the apparent lower volume of fines may have limited the instances of flow fields despite the higher average slopes and a higher predominance of terraces.

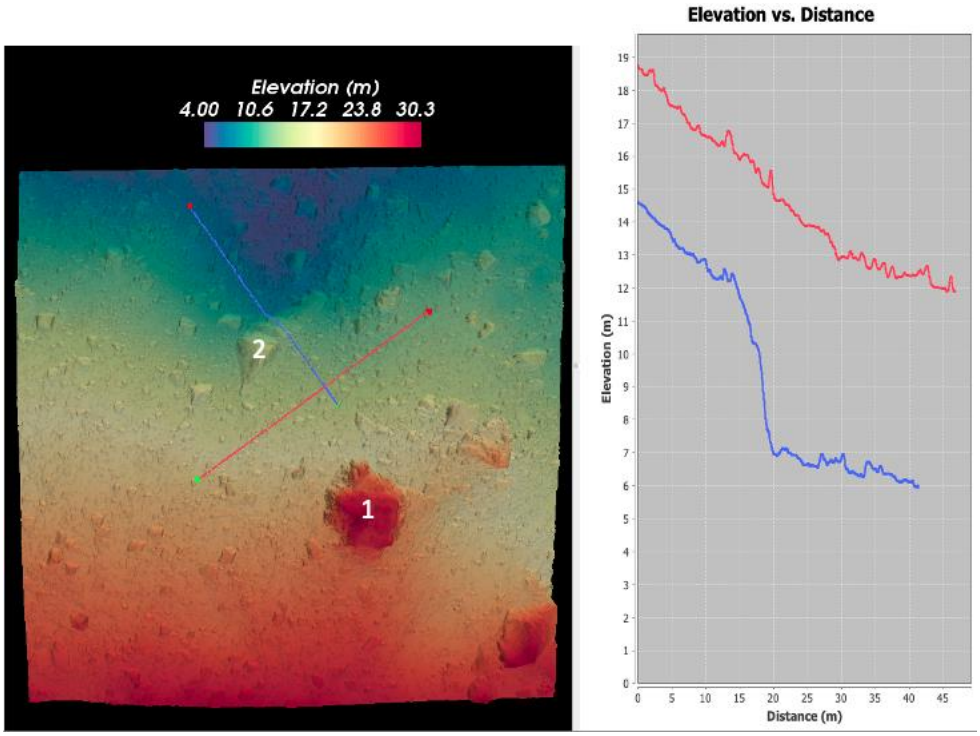

Fig. S1: Laser altimetry topography of the flow field around boulder 2 showing elevations 4 to 5 m lower behind (north) of the bolder. The blue and red lines shown in **a** correspond to the profiles in **b.**

Constraining surface strength

We constrain the possible strength by investigating several parameterizations and placing a value that is likely an extreme but that encloses many of the possible conditions. To set a maximum value on strength of the surface material ejected during formation of Bralgah Crater, we examine the slowest ejecta speeds, which increase as surface strength increases. The slowest ejecta are launched near the crater rim in the final stages of the cratering process. Using one crater radius as the distance that certainly contains ejecta, the minimum deduced ejecta speed is 3.5 cm/s, the speed required to land within one crater radius downslope. (There appear to be ejecta closer than one radius from the crater rim, so this is a conservative speed.) The solid lines in Fig. S2a are the slowest available speeds using the equations for ejecta velocities in Table 1 for different material properties. If surface strength is >20 Pa, then no ejecta for any of the analyzed materials will be sufficiently slow (red line in Fig. S2a) to land as close as 1 crater radius from the rim.

Unfortunately, the slowest ejecta speeds are poorly understood, particularly for low-strength material in microgravity, a regime not available for hypervelocity terrestrial experiments. A common treatment for these slowest speeds is to insert a somewhat-arbitrary factor such as $1-x/R$ into the velocity equation to drive the velocities to zero at the crater edge rather than having the lowest possible speeds truncated at a non-zero value. After adding this factor, we need a different algorithm for finding the lowest velocity to constrain surface strength. We choose an approach based on the total ejected mass: at least 5% of the ejected mass must be slower than the 3.5 cm/s velocity limit. This approach—along with the parameterizations from laboratory experiments—produces the dashed lines in Fig. S2a and increases the maximum possible strength to 100 Pa.

The strength may in fact be much less, but that cannot be discerned from comparing the Bennu observations to the results of terrestrial testing.

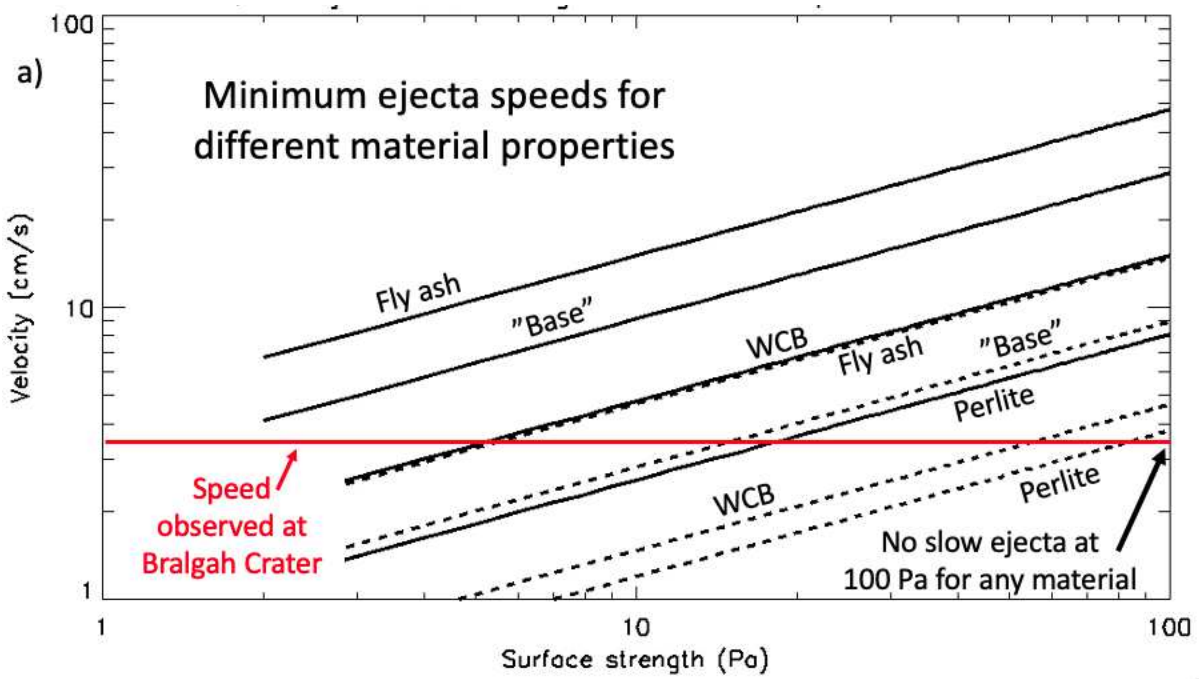

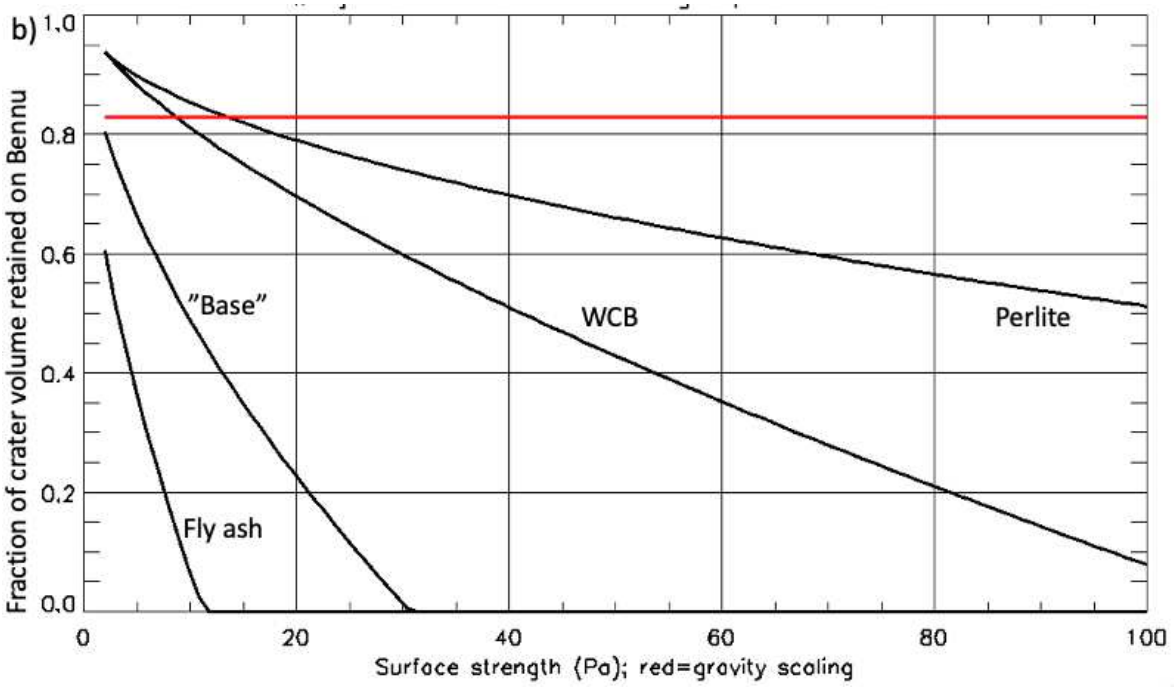

Fig. S2. Calculations of ejecta velocities and the resulting ejected mass using the equations in Table 1 and published parameters[21] for the different material analogs for Bennu's regolith. WCB is weakly cemented basalt, and "Base" has the constant C_3=1 in the strength equation for ejection velocity. **a,** The minimum ejection velocity for the different strength parameterizations. The red line represents the lowest observed speed based on ejecta as close as 1 crater radius from the rim. The solid lines use the Table-1 equations, and the dashed lines include an additional factor that assumes ejecta velocities are not truncated and must

583 smoothly approach zero. Although many of the potential surface properties do not have suf-
584 ficiently slow velocities at 20 Pa, all of the strength parameterizations have high velocities at
585 100 Pa. **b,** Fraction of ejecta retained for a 35 m crater on Bennu as a function of target
586 strength. The red line represents the fraction retained for gravity-regime scaling. For this
587 plot, ejecta are considered retained if their ejection velocity is below 16 cm/s, the escape
588 velocity on Bennu at 45°S. For velocities between 15 and 20 cm/s, retention depends on lo-
589 cation and angle of ejection.
590
591
592
593

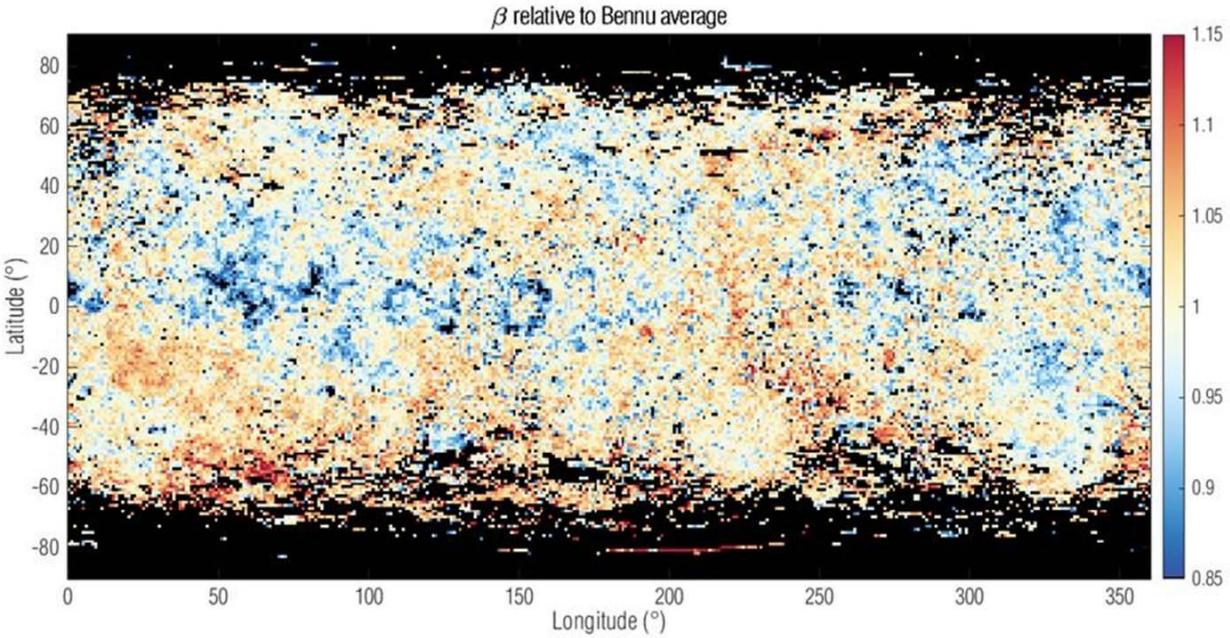

Fig. S3. The colors are the phase slope (Golish et al. 2021) from the linear (in magnitude space) phase function, averaged over 1 degree and normalized to the Bennu average. The underlying data are the PolyCam albedo basemap (Golish et al. 2021). Notionally, low (blue) is a shallower slope and therefore a smoother surface; this is the area north of Bralgah Crater centered at 45°S, 325°E. The scale is –10%/+5%, so the flow region is approximately a 10% effect.

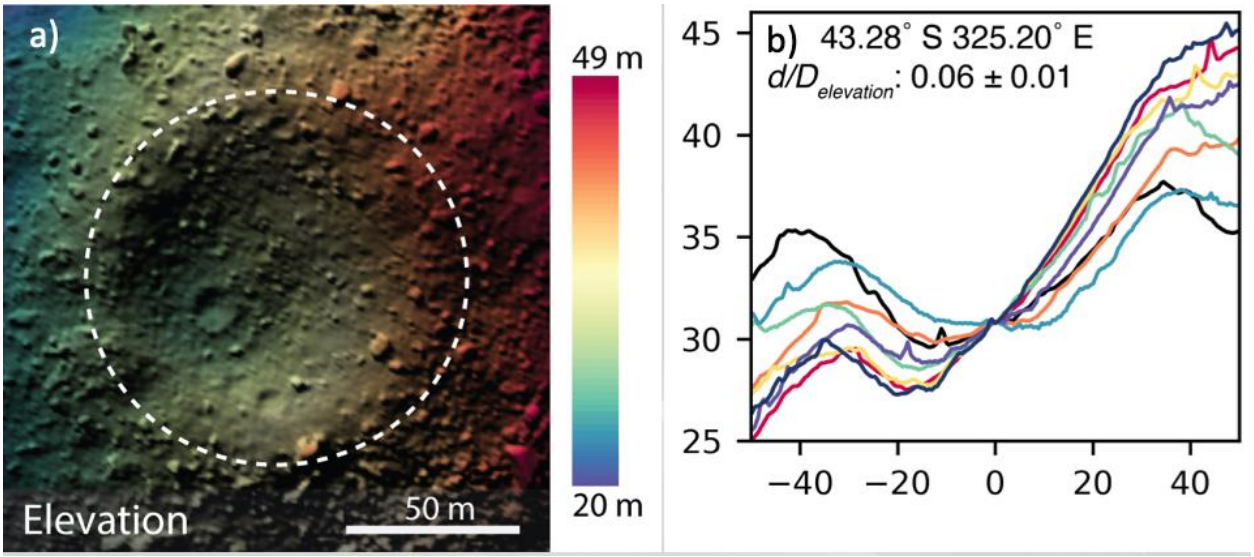

Fig. S4. Topography of Bralgah Crater from laser altimetry data (Figures 1, 2)[14]. Bralgah Crater resides on a slope of ~23°. **a**, DTM overlaid onto an OCAMS image (ocams20190419t204556s223_map_iofl2pan_92585). North (downslope) is to the left. **b**, Eight profiles of the crater. The value $d/D_{\text{elevation}}$ is crater depth (calculated from elevation) divided by crater diameter. The apparent asymmetry is due to the prevailing slope of the local region. Because of compaction and uplift near the crater rim, the total volume of material excavated from an impact crater is typically about 2/3 of the crater volume [21,35].

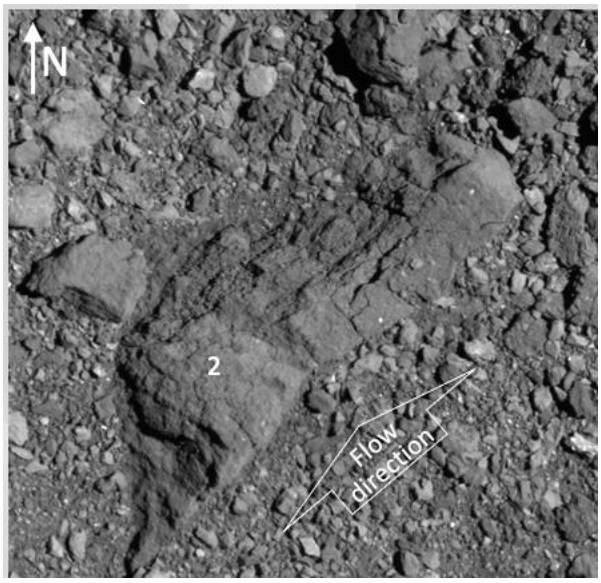

Fig. S5. Higher-resolution view (global mosaic[11]) of boulder 2 indicating that material flowed against the south-east side of the boulder. Figure S1 shows the drop in elevation to the north-west.